

Shear flow instability in the dipolar magnetosphere

I. Voronkov, R. Rankin, J. C. Samson, and V. T. Tikhonchuk¹

Department of Physics, University of Alberta, Edmonton, Alberta, Canada

Abstract. The three-dimensional, nonlinear evolution of a shear flow (or Kelvin-Helmholtz (KH)) instability driven by a large-amplitude shear Alfvén wave (SAW) in the Earth’s magnetosphere is studied by using numerical solutions to the complete set of ideal magnetohydrodynamic equations. An initial setup is chosen to simulate a standing SAW associated with field line resonances (FLRs) in a dipolar magnetosphere. It is shown that KH vortices grow most rapidly in the equatorial plane. In this region, the growth rate is reduced by the ratio of the KH and SAW frequencies when compared to the growth rate predicted by a two-dimensional theory for transient magnetic field lines. For typical parameters of FLRs, this ratio is small. Field-aligned gradients of the KH mode vorticity and azimuthal phase velocity initiate Alfvén waves, which carry energy toward the ionosphere. This results in partial restructuring of field-aligned currents with scale size of ~ 10 km above the ionosphere. After one period of the SAW, energy in the KH mode returns to the SAW flow. This suggests that vortex formation might be largely periodic in evolution, reconfiguring after each period of the FLR. Finally, we show that this restructuring of field-aligned currents does not depend on the initial phase of the SAW. For example, the model predicts that a ground-based observer in the Northern Hemisphere (looking antiparallel to the Earth’s magnetic field) will see that the downward current wraps clockwise and the upward current wraps counterclockwise, though the positions of the currents change latitudes for different phases.

1. Introduction

A commonly observed feature of enhanced auroral activity is the formation of vortical structures. *Hallinan* [1976] classified these forms as spirals (~ 50 km), folds (~ 20 km), and curls (~ 5 km). Recently, similar vortical structures were also observed for fine-structured discrete arcs of the thickness of 0.1–1 km [*Trondsen and Cogger*, 1998] and for black auroras [*Trondsen and Cogger*, 1997]. According to *Miura* [1996, p.764] an “auroral vortex street (curl) often seen in association with discrete auroral arcs is visible evidence of the K-H instability driven by the shear of the $\mathbf{E} \times \mathbf{B}$ drift velocity,” where K-H refers to Kelvin-Helmholtz.

Recently, *Samson et al.* [1996, 1998] showed that some discrete auroral arcs are modulated with frequencies corresponding to field line resonances (FLRs) and have topology compatible with the upward currents expected in FLRs. This implies that large-amplitude FLRs may lead to the formation of some arcs. The velocity field of standing SAWs have nodes in a highly con-

ductive ionosphere and antinodes in the equatorial magnetosphere. In a dipolar magnetic field, FLRs evolve into a radially structured channel in the vicinity of the resonant magnetic L shell [*Streltsov and Lotko* 1996, 1997; *Voronkov et al.*, 1997a]. The velocity gradients increase with time and eventually the FLR may become unstable with respect to the Kelvin-Helmholtz mode [*Rankin et al.*, 1993; *Samson et al.*, 1996, 1998]. The KH mode is expected to develop first near the equatorial plane, driving shear Alfvén waves and field-aligned currents that interact with the ionosphere. In order to find the three-dimensional dynamics of the instability in the magnetosphere, we have studied the evolution of the shear flow within a SAW using a dipolar geometry on a magnetic shell with $L \sim 10$, where active discrete arcs are observed in the evening and midnight ionosphere.

It is well known that if the ambient magnetic field has a component directed parallel (or antiparallel) to the wave vector, the growth rate decreases and such a magnetic field can eventually stabilize KH modes [*Miura and Pritchett*, 1982; *Tajima et al.*, 1991]. The KH instability growth rate also depends on conditions at the ionospheric ends of the magnetic field lines. The influence of ionospheric line tying on the KH instability was studied by *Miura and Kan* [1992], *Galinsky and Sonnerup* [1994], and *Miura* [1996]. It was shown that for a sufficiently large ionospheric conductivity, the line-tying effect suppresses the instability whenever $\gamma < k_{\parallel} V_A$. Here γ is the local instability

¹On leave from the P. N. Lebedev Physics Institute, Russian Academy of Science, Moscow.

growth rate without line-tying effects, k_{\parallel} is the wavelength parallel to the ambient magnetic field, and V_A is a characteristic Alfvén velocity. *Miura* [1996] found a critical value of height-integrated Pedersen conductivity $\Sigma_{P_c} \sim 1/(4\pi V_A)$, which makes the KH mode completely stable at time larger than transient Alfvén time. However, if $\gamma > k_{\parallel} V_A$, the KH mode dynamics in the equatorial magnetosphere is much less affected by the ionosphere because the instability develops faster than the Alfvénic transit time. Some observations show that the characteristic time for the auroral vortex formation is of the order of tens of seconds for folds and curls with a length scale of the order of 10 km [Hallinan and Davis, 1970; Davis and Hallinan, 1976; Hallinan, 1976; Haerendel et al., 1996; Trondsen and Cogger, 1997, 1998]. This time scale is shorter than the field-aligned Alfvén transit time (which is of the order of one hundred seconds for $L \sim 10$). Therefore one can expect that for these structures, the KH instability in the equatorial magnetosphere could initially develop without significant ionospheric effect. The effects associated with the curvilinear topology of the magnetic field lines and ionospheric line tying may become important in a further stage of the KH instability evolution when Alfvén waves have carried vortices associated with the KH instability to the ionosphere. A three-dimensional model of the instability that accounts for the curvilinear topology and finite length of the magnetic field lines is required to describe these vortex dynamics in the magnetosphere and to predict its signatures above the ionosphere.

In this paper, we present the results of computer modeling of a three-dimensional (3-D) KH mode instability within FLRs in a dipolar magnetosphere with plasma parameters compatible with those found on field lines threading the auroral ionosphere. We assume that the shear flow produced by the FLR has a thickness much smaller than the field-aligned length. Our primary goal is to study the nonlinear 3-D dynamics of the KH instability initiated by standing SAWs on dipolar magnetic field lines, to identify mechanisms that can transport energy toward the ionosphere, and to compare results with those obtained by using a simplified analytical model. In this paper, we address the following questions: (1) How does the vortex evolve? (2) What are the effects of the curvature and nonuniform ambient magnetic field that appear owing to the dipolar topology? (3) How does the KH vortex in the equatorial magnetosphere drive field-aligned currents above the ionosphere, and what is the time delay between these structures? (4) What are the processes saturating the instability?

The paper is constructed as follows. In section 2, we describe the magnetohydrodynamic (MHD) dipolar model and the initial setup used for simulations. The analysis of the instability is presented in the third section. A simplified analytical model has been developed to explain the field-aligned interaction between vortices at different altitudes. We consider excitation and dynamics of field-aligned currents, which provide energy transport toward the ionosphere. In the fourth section

we discuss applicability of the model in describing auroral structures and show simplified schematics of field-aligned current dynamics that follow from the model. In the final section, we summarize the results of this study.

2. SAWs in a Dipolar Geometry

The SAW and KH mode dynamics are modeled by using the following set of MHD equations:

$$\frac{\partial \mathbf{B}}{\partial t} - \nabla \times (\mathbf{V} \times \mathbf{B}) = 0, \quad (1)$$

$$\frac{\partial (\rho \mathbf{V})}{\partial t} + \nabla \cdot (\rho \mathbf{V} \wedge \mathbf{V}) = -\nabla P + \frac{1}{4\pi} (\nabla \times \mathbf{B}) \times \mathbf{B}, \quad (2)$$

$$\frac{\partial \rho}{\partial t} + \nabla \cdot (\rho \mathbf{V}) = 0, \quad (3)$$

$$\frac{d}{dt} \left(\frac{P}{\rho^\Gamma} \right) = 0. \quad (4)$$

In these equations, \mathbf{V} is the fluid velocity, \mathbf{B} is the magnetic field, ρ is the plasma density, P is the thermodynamic pressure, and Γ is the adiabatic constant. In the flux equation, \wedge stands for a dyadic product.

For this study, we use dipolar coordinates (μ, ν, ϕ) , where $\mu = \cos\theta/\rho^2$, $\nu = \sin^2\theta/\rho$, and ϕ is azimuthal. The corresponding metrics describe the transform between spherical (ρ, θ, ϕ) and dipolar coordinate systems: $h_\mu = \rho^3/(1 + 3\cos^2\theta)^{1/2}$, $h_\nu = \rho^2/[\sin\theta(1 + 3\cos^2\theta)^{1/2}]$, and $h_\phi = \rho \sin\theta$. The ambient magnetic field is defined as $B_0 = M/h_\mu$, with $M = 8.02 \times 10^{25} \text{ G cm}^3$.

In the simulations, we consider a region extended radially from 9.25 to 10.75 R_E in the equatorial plane and from 1 R_E above the Earth's surface (later referred to as the low altitude boundary (LAB)) to the equatorial plane of the magnetosphere. The boundary above the Earth's surface is assumed at 1 R_E instead of realistic ionospheric altitudes in order to avoid computational problems associated with a sharp gradient of Alfvén velocity near the ionosphere. We shall discuss the validity of this assumption in section 4. Reflection of the Alfvén wave electric field from the ionosphere is defined by the reflection coefficient R [Southwood and Hughes, 1983]. Assuming that V_A is uniform in the ionosphere, this coefficient is $R = (\Sigma_A - \Sigma_P)/(\Sigma_A + \Sigma_P)$, where $\Sigma_A = c^2/(4\pi V_A)$ is the wave conductivity and Σ_P is the height-integrated Pedersen conductivity in the ionosphere. If $\Sigma_P \gg \Sigma_A$, which means that the ionosphere is highly conductive, $R \sim -1$ and incident and reflected electric fields cancel each other. This corresponds to the perfect reflection of Alfvén waves from the ionosphere. Finite ionospheric conductivity $\Sigma_P > \Sigma_A$ results in the partial absorption of the wave energy and a broader FLR. The case $\Sigma_P = \Sigma_A$ corresponds to total absorption. In the auroral ionosphere, Σ_A is of the order of 1-3 S whereas $\Sigma_P > 10$ S. For these parameters, $R < -0.7$ and therefore, the ionospheric boundary is highly re-

flecting. Detailed study of the ionospheric conductivity influence on FLRs was presented by Rankin *et al.* [1999] who showed that a typical damping time is larger than 50 min for $\Sigma_P > 10$ S. This corresponds to ~ 10 periods of typically observed FLRs. In this study, we consider processes that occur within one period of the FLR. Therefore we assumed the LAB to be perfectly reflecting for shear Alfvén waves. This boundary condition leads to a fundamental mode FLR that has an antinode of the magnetic field at the LAB and a node in the equatorial plane of the magnetosphere. Corresponding velocity fields have a node at the LAB and an antinode in the equatorial plane. In this study, we concentrate on a fundamental field-aligned standing FLR mode and its instability with respect to KH modes. In the azimuthal direction, we assume FLR amplitude to be uniform, which corresponds to small- m (large azimuthal wavelength) FLRs. Azimuthal boundary conditions are periodic. The azimuthal length corresponds to one wavelength of the KH mode. The radial boundaries are positioned far away from the perturbed area in order to minimize their influence on wave dynamics. We assume fields at radial boundaries to be evanescent.

The initial geometry is illustrated by Figure 1a, which shows a magnetic L shell from the Earth's surface to the

equatorial plane of the magnetosphere. The dipolar coordinates (μ, ν, ϕ) are directed as follows: μ is directed along magnetic field lines, ν is perpendicular to magnetic field lines and positive Earthward in the equatorial magnetosphere, and ϕ is positive westward.

The background density distribution is $\rho_0 = \rho_{eq}(1 - \cos^2 \theta)^{-q}$, with $\rho_{eq} = 1.044 \times 10^{-24}$ g cm $^{-3}$ and $q = 4$. This density distribution models large-scale density variations along the field lines and is often used for FLR models [Allan and Knox, 1979; Taylor and Walker, 1984]. The eigenvalue analysis shows that the eigenstructure of the FLR depends mainly on the density in the equatorial plane, whereas the dependence on the field-aligned distribution, particularly near the ionosphere, is minimal. For the chosen parameters, the period T of the first fundamental FLR mode at $L = 10$ is 248 s. The plasma pressure P_0 is 0.1 nPa, and it is uniform in the computational volume. This pressure corresponds to $\beta = 8\pi P_0/B_0^2 = 0.28$ at $L = 10$ in the equatorial plane.

The azimuthal magnetic field of the FLR is defined as

$$B_\phi = B_0^{eq} \frac{h_{\phi,eq}}{h_\phi} b(\nu) S(\mu) \cos \omega t, \quad (5)$$

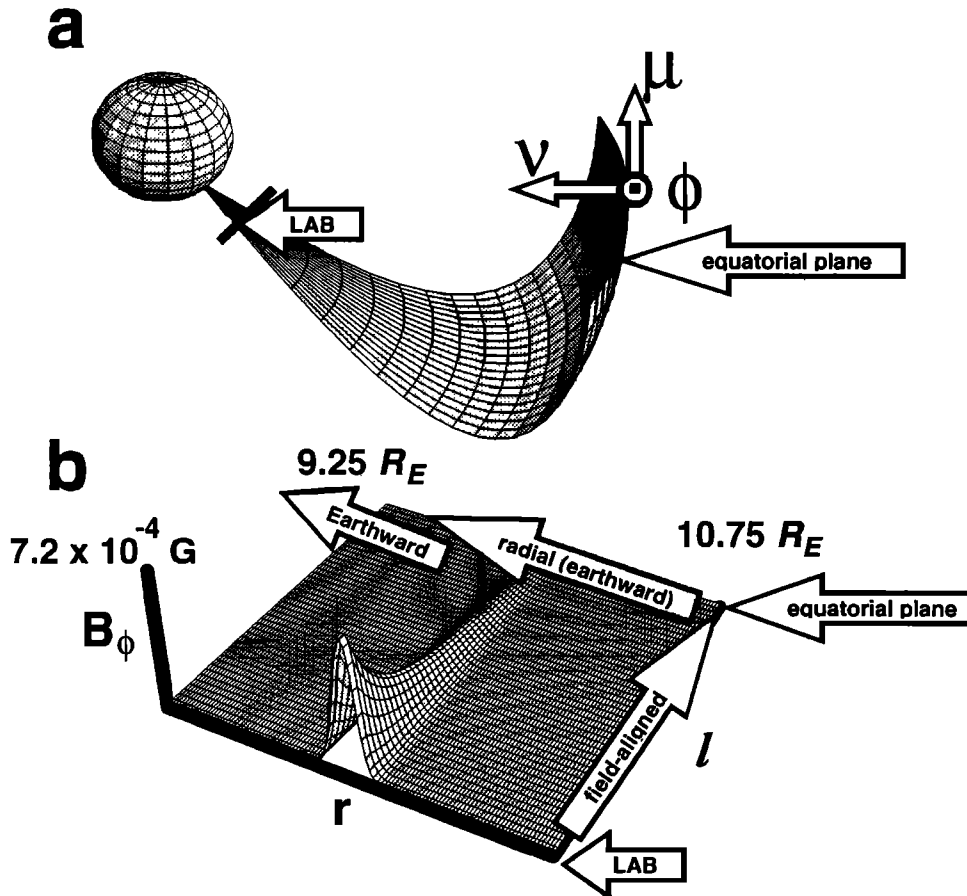


Figure 1. Schematic of the dipolar model geometry illustrating (a) a magnetic L shell and (b) the initial shear Alfvén wave (SAW) magnetic field distribution along magnetic field lines (l direction) and in the radial direction (r direction). The transform between the Cartesian l, r and dipolar μ, ν coordinates is described in the text. LAB is low-latitude boundary.

where B_ϕ is the azimuthal component of magnetic field, B_0^{eq} is the ambient magnetic field in the equatorial plane, $h_{\phi,eq}$ is a value of h_ϕ in the equatorial plane, $b(\nu)$ describes the radial structure of the SAW, and $S(\mu)$ and ω are the field-aligned eigenfunction and eigenfrequency of the fundamental FLR harmonic, respectively. These eigenfunction and eigenfrequency are defined by the eigenvalue equation [Taylor and Walker, 1984]:

$$-\omega^2 S = \frac{h_\phi}{h_\nu} \frac{\partial}{\partial l} \left(V_A^2 \frac{h_\nu}{h_\phi} \frac{\partial S}{\partial l} \right), \quad (6)$$

where $V_A^2 = B_0^2/4\pi\rho_0$ is the square of the background Alfvén speed, l is the distance along the magnetic field line, $dl = h_\mu d\mu$, and l varies from the lower boundary to the equatorial plane along the magnetic field line. The boundary conditions for the fundamental SAW mode are $S(l_{eq}) = 0$ and $\partial S(l_{LAT})/\partial l = 0$. $S(l)$ is normalized as $\int dl (h_\nu/h_\phi) S^2 = L^2 R_E^2$. Our initial conditions for the FLR correspond to the phase when the SAW magnetic field has its maximum value and the azimuthal velocity is zero.

Dealing with a narrow region near the resonance shell $L = 10$, it is convenient to introduce the radial coordinate $r = 1/\nu_0 - 1/\nu$, where $\nu_0 = 1/(10 R_E)$. The initial radial distribution of the azimuthal magnetic field was chosen to be a Gaussian function, $b(r) = b_0 \exp(-r^2/\delta^2)$, with a half width $\delta = 0.0425 R_E$. The radial width of a SAW corresponds to the width of the shear flow in the FLR region according to the calculations by Voronkov *et al.* [1997a] and Samson *et al.* [1998]. The amplitude of the SAW magnetic field is $b_0 = 0.18$, which gives $B_\phi = 72$ nT at the LAB. The initial distribution of B_ϕ in the meridional cross section is shown in Figure 1b. Note that the initial B_ϕ according to (1) does not depend on ϕ .

This azimuthal magnetic field perturbation corresponds to the SAW azimuthal flow

$$V_\phi = \frac{V_A^2 b}{\omega} \frac{h_\nu}{h_{\nu,eq}} \frac{\partial S}{\partial l} \sin \omega t, \quad (7)$$

with the maximum velocity $V_{\phi 0} \simeq 180$ km s⁻¹ in the equatorial magnetosphere, which is in agreement with observations of FLRs. According to the 2-D theory of the KH instability, the chosen width and amplitude of the shear flow provide e -folding time of the vortex formation in the equatorial plane of the order of 10 s, which is smaller than the half period of the SAW.

Beside the toroidal SAW, we also initiate a small perturbation of the radial velocity, which is used as a “seed” for the KH instability. This perturbation was defined as $V_\nu^0 = V_{\nu 0} [h_\phi B_0]_{eq} / (h_\phi B_0) \exp(-r^2/\delta^2) \sin(m\phi)$ with the azimuthal wavenumber $m = LR_E/\delta \gg 1$, the amplitude $V_{\nu 0} = 3$ km/s (which is approximately 1.7% of the maximum SAW azimuthal shear flow velocity), and the same Gaussian distribution of V_ν in the radial direction as for the SAW amplitude. The choice of the azimuthal wavenumber m was made using the simplified KH theory for the transverse magnetic field [Miura and Pritchett, 1982], which predicts the fastest growth rate for this mode in the equatorial plane. The field-aligned

profile of $V_\nu^0(l)$ was designed to minimize coupling to the poloidal SAW modes. Namely, $h_\phi V_\nu^0 B_0$ is constant along the magnetic field line. In linear approximation, (1) for B_ν reads $\partial B_\nu / \partial t = (1/h_\phi)(\partial/\partial l) h_\phi V_\nu B_0$. Therefore our choice of $V_\nu^0(l)$ does not excite the linear poloidal SAW mode in the dipolar topology. This profile of $V_\nu^0(l)$ is equivalent to the uniform field-aligned distribution of the radial velocity in box models.

We continue our simulations for approximately one SAW period. As we show later, the KH mode grows and saturates during the first half period of the SAW. This time interval corresponds to the growth and decay of the SAW azimuthal velocity. After one period of the SAW, the radial perturbation becomes small and the saturated KH mode does not significantly affect the SAW.

3. Excitation and Growth of the Shear Flow Instability of a SAW

The width of shear flows associated with discrete arcs is much smaller than the length of the field lines and $\gamma \gg k_\parallel V_A$. Therefore we can expect that, initially, the shear flow instability in the equatorial plane evolves without significant effects related to the finite magnetic field line length. This allows us to apply a 2-D theory of the KH instability and account for the 3-D evolution of vortices and their field-aligned interaction as a perturbation. Therefore we begin with comparisons of the results of 3-D simulations with predictions of the 2-D theory and simulations.

The distribution of V_ν in (ν, ϕ) planes (perpendicular to the field line) is shown in Figure 2 for different distances along the field line at $t = 20$ s corresponding to the initial growth of the KH mode. An eigenfunction of the KH V_ν predicted by the 2-D linear theory for parameters corresponding to the equatorial plane is shown in Figure 2d. Figure 2 suggests that the 2-D theory of the KH instability provides an appropriate prediction for the initial KH mode excitation in the dipolar 3-D geometry.

In Figure 3, the effective growth of the 3-D KH mode is compared with the predictions of the 2-D theory. For Figure 3, the growth of V_ν is averaged over the time interval $[0; T/4]$ as $1/(T/4) \int_0^{T/4} \gamma dt$, which corresponds to the growth of the azimuthal shear flow. Here γ is a local growth rate computed as $d(\ln V_{\nu, max})/dt$. As seen from Figure 3, the growth rate of the 3-D KH instability is smaller in the equatorial region and larger near the LAB than the growth rate computed using the theory that neglects the effect associated with the finite field line length (2-D theory). As we show later, this occurs owing to the energy exchange between vortices at different altitudes provided by the 3-D KH current system. In spite of quantitative difference, Figure 3 demonstrates that the field-aligned distribution of the 3-D KH mode growth rate is in qualitative agreement with the linear 2-D theory predictions.

These results show that for chosen parameters, the 3-D KH instability initially evolves in a fashion similar

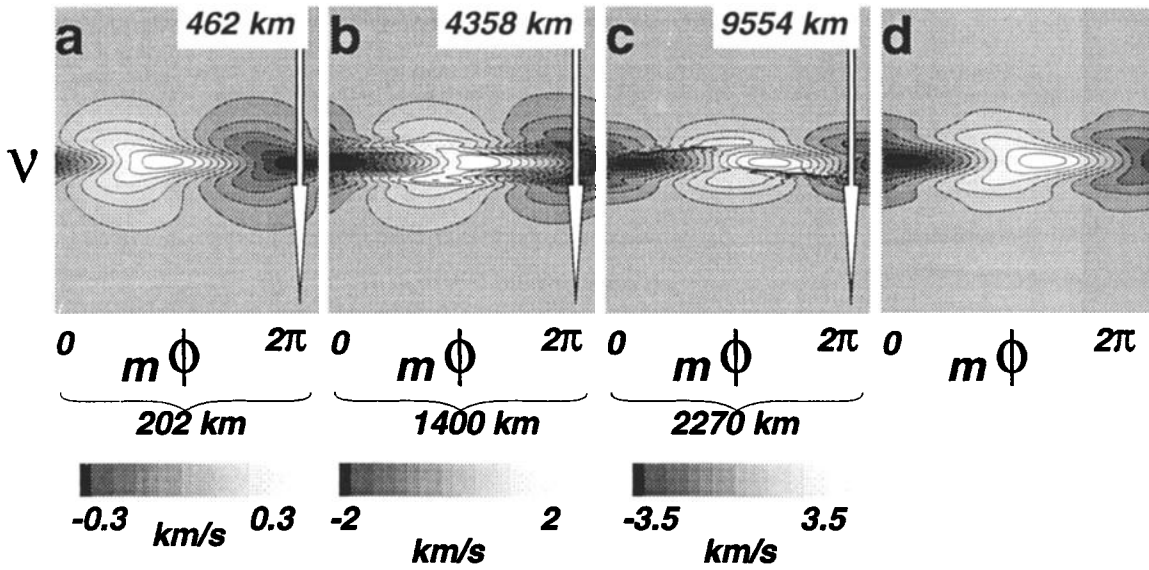


Figure 2. Radial (ν) and azimuthal (ϕ) distribution of the radial flow velocity V_r at $t = 20$ s at altitudes (a) $1 R_E$, (b) $6 R_E$, and (c) $12 R_E$ above the LAB along the field line and (d) a Kelvin-Helmholtz (KH) eigenmode $V_r(r, \phi)$ predicted by the 2-D theory at $12 R_E$ for $q\delta = 1$ (arbitrary units). Arrows indicate the radial scales of Figures 2a - 2c, and azimuthal scales are shown below.

to the 2-D KH instability. However, in the 3-D case, there is a field-aligned interaction (or energy exchange) between vortices at different altitude levels. This interaction should be accounted for in order to obtain more accurate growth rates of the 3-D instability. Below, we develop a simplified analytical model of the KH instability in the dipolar coordinates, which can explain the field-aligned vortex coupling in terms of currents produced by the instability.

Owing to the fact that the radial scale of the SAW is smaller than field-aligned scale sizes, the governing equations for the SAW can be reduced from the general form (1)-(4) to equations for the electrostatic potential Φ and the parallel component of the vector potential A :

$$\frac{d}{dt} \nabla_{\perp}^2 \Phi = -\frac{V^2}{c} \nabla \cdot (\mathbf{b} \nabla_{\perp}^2 A), \quad (8)$$

$$\frac{1}{c} \frac{dA}{dt} = -(\mathbf{b} \cdot \nabla) \Phi, \quad (9)$$

where d/dt is the full (including the convective term) time derivative and \mathbf{b} is the unit vector in the direction of the total magnetic field. Equation (8) describes the current continuity in the system, and (9) is the condition for the zero parallel electric field [Strauss, 1976; Petviashvili and Pokhotelov, 1985].

Assuming fields independent of the azimuthal coordinate, linearized equations (8)-(9) describe a standing SAW:

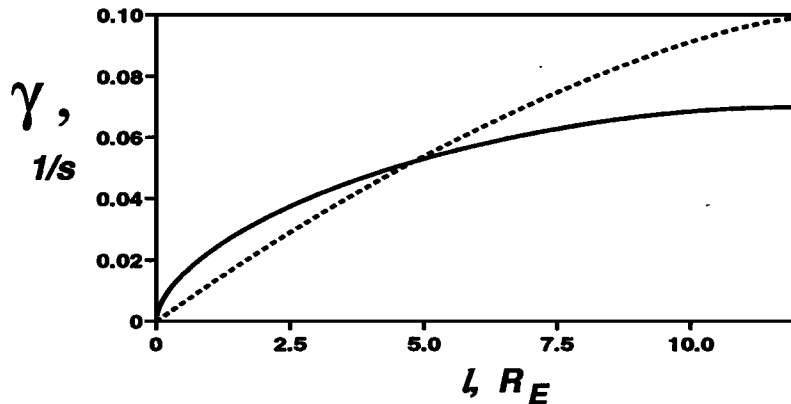


Figure 3. Field-aligned distribution of the KH instability growth rate (averaged over $1/4$ of the SAW period) obtained from the 3-D simulations (solid line) and as predicted by the 2-D linear theory (dashed line). Here l varies from the LAB to the equatorial plane along the magnetic field line.

$$\frac{\partial}{\partial t} \Phi_0 = -V_A^2 \frac{h_\nu}{ch_\phi} \frac{\partial}{\partial l} \frac{h_\phi}{h_\nu} A_0, \quad (10)$$

$$\frac{1}{c} \frac{\partial A_0}{\partial t} = -\frac{\partial \Phi_0}{\partial l}, \quad (11)$$

with $B_\phi = -(1/h_\nu)(\partial A_0/\partial \nu)$ and $V_\phi = (c/B_0 h_\nu) \times (\partial \Phi_0/\partial \nu)$ defined by (5) and (7).

We consider stability of the SAW shear flow with respect to azimuthal perturbations. Let us assume that A_0 and Φ_0 depend on l and t slowly compared to the local KH growth rate $\gamma \gg \omega$. In this case, the electric and magnetic potentials can be presented in the form $A = A_0 + \delta A$ and $\Phi = \Phi_0 + \delta \Phi$, where δA and $\delta \Phi$ are small corrections due to the KH mode excitation. We can also assume that δA and $\delta \Phi$ are proportional to $\exp(-i \int \Omega dt + im\phi)$, where Ω is the instantaneous KH mode frequency and $\gamma = \text{Im}\Omega$. Because of a slow variation of SAW potentials Φ_0 and A_0 along the magnetic field line, we can adopt a perturbation theory approach. For the zeroth-order approximation, we neglect all derivatives along the magnetic field line and construct a 2-D KH mode solution $\delta \Phi^{(0)}$, $\delta A^{(0)}$, and $\Omega^{(0)}$. Then we shall find $\delta \Phi^{(1)}$, $\delta A^{(1)}$, and $\Omega^{(1)}$ corrections due to the field-aligned inhomogeneity.

Neglecting the right-hand side of (8), which contains the derivative along the magnetic field line, one can obtain a zero-order eigenmode equation for the KH instability:

$$\frac{d^2}{d\nu^2} \delta \Phi^{(0)} = \left[q^2 h_\nu^2 - \frac{q V_\phi''}{\Omega^{(0)} - q V_\phi} \right] \delta \Phi^{(0)}, \quad (12)$$

where $V_\phi'' = d^2 V_\phi / d\nu^2$, $q = (m/h_\phi)$ is the azimuthal wave number and V_ϕ is the SAW azimuthal velocity described by (7). This equation defines a complex frequency of KH mode $\Omega^{(0)}(l, t)$ in dipolar coordinates. This frequency is a slow function of l and t because the shear flow velocity and q vary along the magnetic field lines and change in time. Equation (12) describes a local 2-D KH instability. It has an unstable solution $\text{Im}\Omega^{(0)} > 0$ for $q\delta \lesssim 1.9$. Its eigenfunction for $V_\nu = -imc\delta\Phi^{(0)}/B_0 h_\phi$ is shown in Figure 2d for $q\delta = 1$, which corresponds to the highest KH growth rate.

In the next order, (9) defines a vector potential associated with the KH instability

$$\delta A^{(1)} = -\frac{c\delta\Phi^{(0)}}{\Omega^{(0)} - qV_\phi} \frac{\partial}{\partial l} \int \Omega^{(0)} dt, \quad (13)$$

and the radial component of the magnetic field $B_\nu = (im/h_\phi)\delta A^{(1)}$. Note that the magnetic potential and B_r exhibit a secular growth in time and might have a significant effect on the KH instability after the Alfvén transit time.

Substituting (13) into (8), one can find an equation for the KH instability that accounts for the energy exchange along magnetic field lines. In particular, it provides for the following correction to the KH mode eigenfrequency:

$$\Omega^{(1)} = \alpha \frac{V_A^2}{\Omega^{(0)}} \left[i \frac{h_\nu}{h_\phi} \frac{\partial}{\partial l} \left(\frac{h_\phi}{h_\nu} \frac{\partial}{\partial l} \int \Omega^{(0)} dt \right) + \left(\frac{\partial}{\partial l} \int \Omega^{(0)} dt \right)^2 \right] \quad (14)$$

Here the coefficient α accounts for the radial structure of the KH mode eigenfunction:

$$\alpha = \frac{\Omega^{(0)} \int d\nu [(G')^2 + q^2 h_\nu^2 G^2]}{\int d\nu (q V_\phi'' G^2)}, \quad (15)$$

where

$$G = \frac{\delta \Phi^{(0)}}{\Omega^{(0)} - q V_\phi}. \quad (16)$$

For our parameters $q\delta = 1$, the coefficient $\alpha = 0.19 - 0.51i$.

As seen from (14), the correction to the KH growth rate arises owing to field-aligned variations of $\Omega^{(0)}$. These variations produce field-aligned currents and Alfvén waves that transfer the KH mode energy from the equatorial plane toward the ionosphere. Let us estimate the frequency correction (14) near the equatorial plane where the KH growth rate has a maximum. Because $\Omega^{(0)}$ is an even function of l with respect to the equator, $\partial \Omega^{(0)}/\partial l$ goes to zero in this region, the first term in the square brackets dominates, and $\Omega^{(1)}$ can be estimated as

$$\Omega^{(1)} \sim \alpha \frac{V_A^2}{L^2 R_E^2 \omega} \sim \omega. \quad (17)$$

For our set of parameters, this estimate gives a correction to the growth rate of the order of 25%, which is in agreement with the numerical result shown in Figure 3. As seen from (16), the frequency correction in the equatorial plane is small whenever the KH frequency is larger than the SAW frequency, which is consistent with the original assumption made for this derivation.

It is interesting to note that the field-aligned propagation of the KH perturbation occurs in the form of the oblique wave as shown in Figure 4. This happens owing to the field-aligned inhomogeneity of the KH mode phase velocity because of the nonuniform field-aligned distribution of the KH mode frequency and wavelength. As a result, vortices at different altitudes move in azimuthal direction with respect to each other, which eventually leads to a significant azimuthal shift between perturbations at different altitudes.

The nonuniform distribution of the velocity perturbation along the magnetic field line causes perturbations in the radial and azimuthal magnetic field components owing to restructuring of the current system. These magnetic field perturbations reflect the field-aligned current structure above the ionosphere, which may be of a particular interest with respect to comparisons with observations of auroral arcs. According to (13), the amplitude of the radial magnetic field exhibits secular growth in time. After $t \sim T/4$, the magnetic energy of the KH vortex becomes comparable with its kinetic

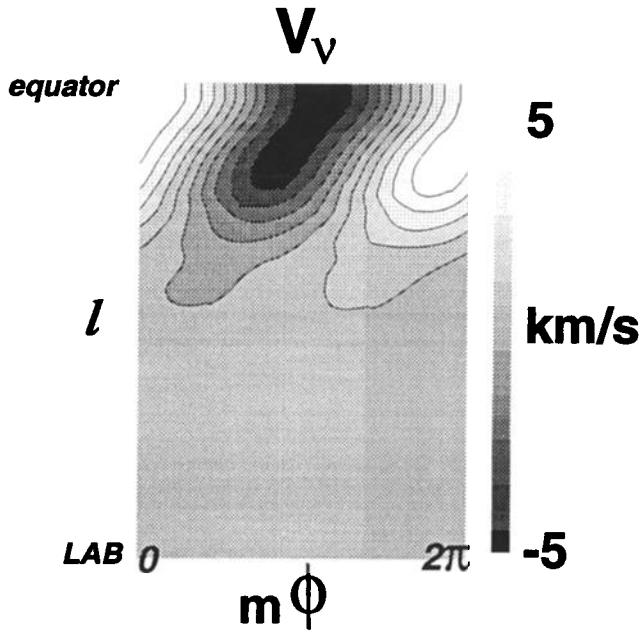


Figure 4. Field-aligned (l) and azimuthal (ϕ) distribution of the radial flow velocity V_v at $t = 25$ s on L shell 10.

energy. Then the field-aligned currents associated with the KH vortex become comparable with the eigenmode FLR current:

$$\begin{aligned} \delta j_{\parallel}^{(1)} &= -\frac{c}{4\pi} \left(\frac{1}{h_v^2} \frac{\partial^2}{\partial \nu^2} - \frac{m^2}{h_\phi^2} \right) \delta A^{(1)} \sim j_{\parallel 0} \\ &= -\frac{c}{4\pi h_v^2} \frac{\partial^2}{\partial \nu^2} A_0. \end{aligned} \quad (18)$$

Temporal variations of the field-aligned current amplitude above the ionosphere are illustrated in Figure 5 for the SAW (independent of ϕ) and KH vortex components of j_{\parallel} . Initially ($t < T/4$), the field-aligned current associated with the KH vortex grows secularly (linearly

in time), as discussed above. Then the growth of the KH field-aligned current is defined by the field-aligned gradient of the vortex amplitude. Owing to the oblique propagation of the KH vortex energy, this gradient also contributes to the current exchange between the SAW and KH modes. After $t \sim T/2$, the KH mode field-aligned current saturates. For our parameters, the initial amplitude of the SAW field-aligned current is $3.8 \mu\text{A m}^{-2}$, and approximately half of this current transforms into the azimuthally structured KH mode current. These currents are compatible with those observed above auroral structures.

The spatial distribution of field-aligned currents above the ionosphere is shown in Figure 6 for different moments of time: $t = 50, 75, 100, 125,$ and 235 s. Initial distribution consists of a system of upward and downward current sheets $j_{\parallel 0}$ produced by the SAW, which do not have azimuthal modulation. The instability leads to the formation of the wave-like structure ($t = 75$ and 100 s), which moves in the azimuthal direction. Later, this structure grows ($t = 125$ s) and disappears ($t = 235$ s).

Figure 7 shows the evolution of the vorticity $(\nabla \times \mathbf{V})_{\parallel}$ in the equatorial plane. As seen from Figure 7, initially, the vortex dynamics are similar to those in the two-dimensional instability of the shear flow in the transient magnetic field [e.g., *Voronkov et al.*, 1997b, Figure 7b]. After the first $1/4$ period, V_0 achieves its maximum and then decreases to zero at $t = 124$ s. At this time, the growth of the radial velocity amplitude ceases, the vortex extends in the radial direction, and its amplitude gradually decreases.

Comparing Figures 6 and 7, one can see that the field-aligned current structure above the ionosphere is a response to the vortex dynamics in the equatorial magnetosphere. The time delay of this response is approximately equal to the the Alfvén propagation time from the equatorial plane to the ionosphere. In our model, this time is ~ 60 s for toroidally polarized waves and ~ 50 s for the poloidally polarized waves. Therefore the field-aligned current distribution at $t = 125$ s is a response to the $(\nabla \times \mathbf{V})_{\parallel}$ structure at $t = 75$ s. Sat-

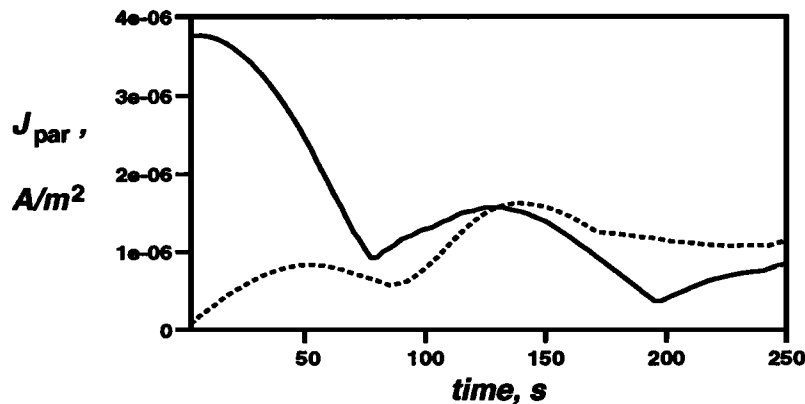


Figure 5. Temporal evolution of the field-aligned current amplitude associated with the field line resonance (FLR) mode (solid line) and KH mode (dashed line).

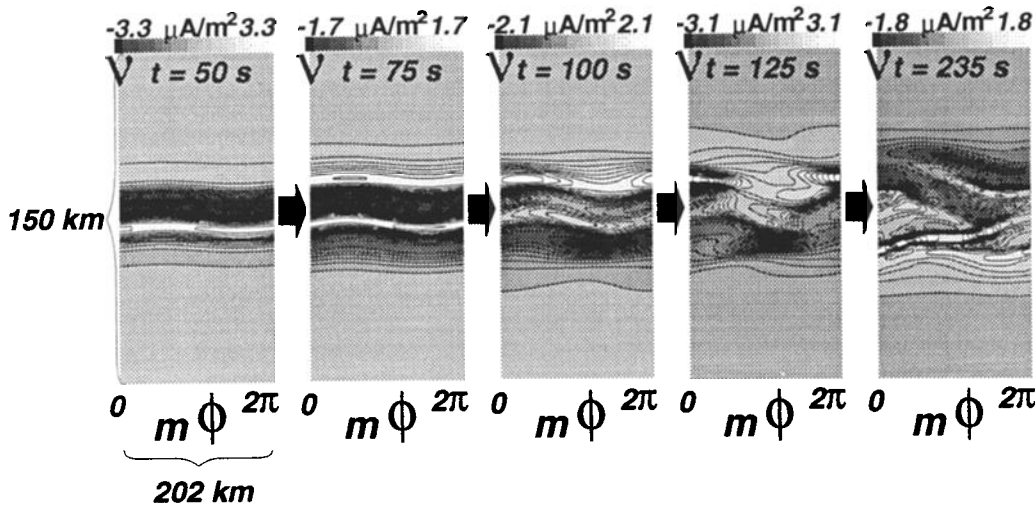


Figure 6. Time slices of the field-aligned current distribution above the ionosphere at $t = 50$, 75, 100, 125, and 235 s.

uration and azimuthal stretching of vortical structure in the equatorial plane shown in Figure 7 for $t = 175$ s lead to the radial narrowing and azimuthal stretching of field-aligned currents as shown in Figure 6 for $t = 235$ s.

Temporal evolution of the KH mode energy normalized by the total energy of the initial SAW is shown in Figure 8. Initially, the growth of the KH mode energy is provided by the vortical structure development in the equatorial magnetosphere. After $\sim T/4$, the vortex saturates and stored kinetic energy transforms into the magnetic energy of the KH mode, which reaches its maximum after $\sim T/2$ and then decreases because the shear flow changes its direction and the KH vortex energy transforms back into the SAW shear flow. This energy exchange obtained numerically is in agreement with analytical predictions discussed above. The sec-

ond maximum of the kinetic energy appears owing to the excitation of new KH instability with the reverse direction of the shear flow. This new KH vortex has an opposite direction with respect to the initial KH mode. Therefore its kinetic energy grows to the lower level with almost no contribution to the magnetic energy of the system.

The energy exchange between the SAW and vortices causes the broadening and partial dissipation of the shear flow within SAW. Figure 9 shows time evolution of the radial distribution of the value $\int_0^{2\pi} V_\phi d\phi$ in the equatorial plane, which characterizes an average mass transport by the FLR azimuthal shear flow. The broadening of the shear flow is similar to the result found by Rankin *et al.* [1997] using the box model. This broadening and partial dissipation of the flow is principally a 3-D KH effect, which occurs owing to the spatial local-

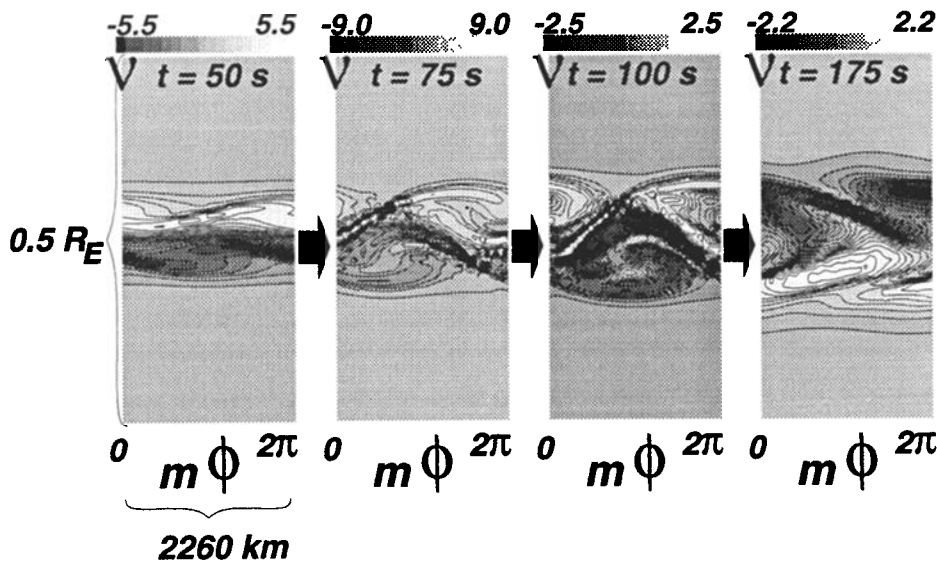


Figure 7. Time slices of the field-aligned component of the vorticity $(\nabla \times V)_\parallel$ in the equatorial plane at $t = 50$, 75, 100, and 175 s. Gray scale numbers are normalized by 10^8 s.

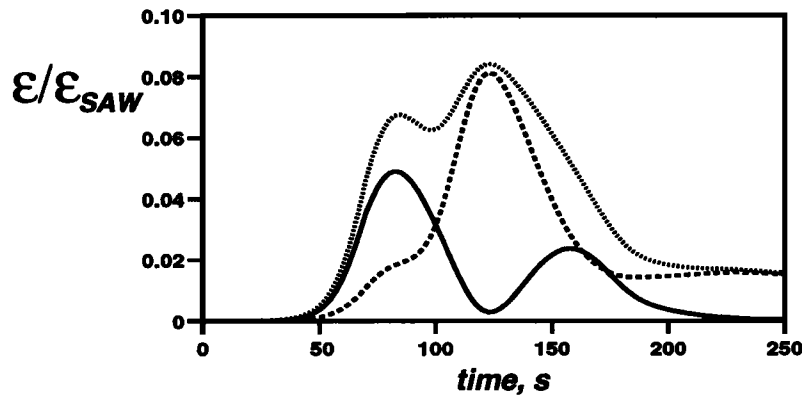


Figure 8. Temporal evolution of the kinetic energy (solid line), magnetic energy (dashed line), and total energy (dotted line) of the KH mode. All values are normalized by the total energy of the initial SAW.

ization of the shear flow along the magnetic field lines. In the 2-D case, the flow periodically widens and narrows with a period equal to the KH instability growth time [Rankin *et al.*, 1997].

4. Discussion

In this paper, we have presented a three-dimensional, nonlinear model of the shear flow instability, which may occur in the some types of auroral arcs that are associated with FLRs. This model was constructed using a dipolar coordinate system. It takes into account the curvilinear magnetic field in the magnetosphere and allows for nonuniform Alfvén velocity distribution along field lines and across magnetic L shells.

Our study is devoted to the KH modes with radial and azimuthal characteristic scale sizes much smaller than magnetic field line lengths. Radially narrow flow channel of high velocity in FLRs can provide $\gamma > k_{\parallel} V_A$. Qualitatively, we have used the characteristic structure of FLRs that appear in the evening and midnight regions. In this case, the stabilizing effect of finite field line length bounded by the ionosphere with finite Pedersen conductivity [Miura and Kan, 1992; Galinsky and Sonnerup, 1994; Miura, 1996] is small, and large-amplitude 3-D KH modes can be excited. The maximum amplitude of the KH vortex is defined by the amplitude and duration of unidirectional SAW flow, and we observe periodic energy exchange between KH and SAW modes.

Some physical effects have been neglected in this study. In this modeling, we have adopted an MHD model that does not account for kinetic or finite Larmor radius effects. For the chosen SAW and density distribution, the ion Larmor radius and electron inertia length are smaller than the scale size of the KH mode. However, for smaller structures, kinetic effects should be taken into account. Kinetic and fluid-kinetic hybrid models of the KH instability have been presented by Ganguli *et al.* [1988], Thomas and Winske [1993], and Huba [1996]. These studies showed the importance of small-scale effects and their influence on the growth rate

and frequency of the KH instability. Ultimately, the electron inertia results in small-scale restructuring of large-amplitude SAWs in FLRs and leads to the energy dissipation from the SAW [Wei *et al.*, 1994; Streltsov and Lotko, 1996; Rankin *et al.*, 1999]. These effects may be valid for the auroral arc fine structure dynamics and may be considered as an important direction toward a comprehensive auroral arc model. We have ne-

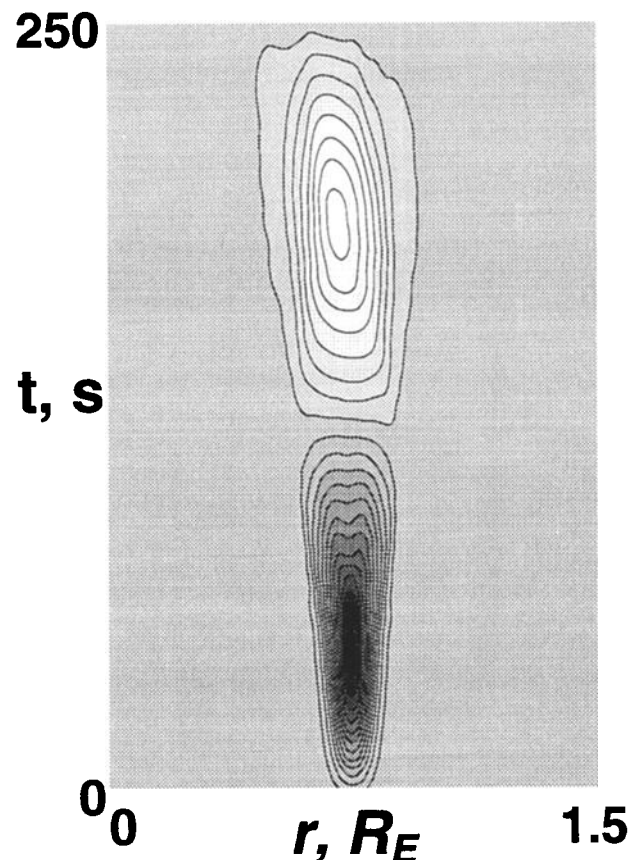


Figure 9. Temporal evolution of the azimuthal shear flow produced by the SAW in the equatorial plane as obtained from the 3-D simulations.

glected strong gradients of Alfvén speed near the ionosphere [Lysak and Carlson, 1981; Trakhtengerts and Feldstein, 1984, 1991; Lysak, 1988, 1991]. Although this strong inhomogeneity may affect the longitudinal structure and long-term dynamics of standing SAWs, they cannot have any significant influence on the KH mode evolution, which occurs in the time interval less or comparable to the Alfvén transit time.

Our model based on the MHD approach predicts the generation and restructuring of field-aligned currents above the ionosphere. Partial transforming of these field-aligned currents into particle fluxes due to kinetic wave-particle interactions lies beyond the scope of our model. Recent studies by Lysak and Lotko [1996] have suggested that acceleration mechanisms such as Landau damping cannot significantly modify or saturate SAWs with a transverse width larger than the ion Larmor radius during a timescale that is smaller than the ion acoustic wave period, which is justified for our model. Namely, the structure should be of the order of kilometers or larger at the ionospheric level.

In the framework of our model, we can assume that a field-aligned potential drop that accelerates particles is directed in such a way that a bright auroral structure corresponds to upward field-aligned currents (or the dark aurora would appear in the region of the downward current) with current densities above an established threshold ($\sim 1 \mu\text{A m}^{-2}$ or greater). Following the model, let us consider the arc dynamics during one period of the FLR. These dynamics are schematically illustrated in Figure 10, which shows two half periods of the SAW when the flow in the equatorial magneto-

sphere (top panels) is westward (Figure 10a) and eastward (Figure 10b). The corresponding ionospheric current structure response (bottom panels), which occurs with a time delay equal to a quarter of the SAW period, is shown for the Northern Hemisphere footprint of the magnetic field lines. The westward shear flow in the equatorial plane drives an azimuthally stretched field-aligned current structure in which the upward current maps poleward from the downward current. Ionospheric footprints of upward and downward field-aligned currents are shown in Figure 10 as open and solid bands, respectively. The unstable KH mode causes restructuring of the vorticity in the equatorial plane. The tailward part of the shear flow wraps clockwise, whereas the earthward part of the shear flow wraps counterclockwise viewed in the direction of the magnetic field. This causes the corresponding wrapping of the field-aligned current structure. In the Northern Hemisphere, a ground-based observer looking upward will see that the upward field-aligned current wraps counterclockwise and the downward field-aligned current wraps clockwise. After half a period of the SAW, this structure changes in the equatorial magnetosphere and a channel of eastward flow in the FLR starts growing. This flow drives a new field-aligned current system with the downward current lying poleward from the upward current, as shown in Figure 10b. The wrapping of the SAW in the equatorial plane is opposite to what it was for the first half period. However, owing to the change of the field-aligned current system, the ground-based observer will find that when correlated with visible aurora, this wrapping is directed in the same fashion as for the first

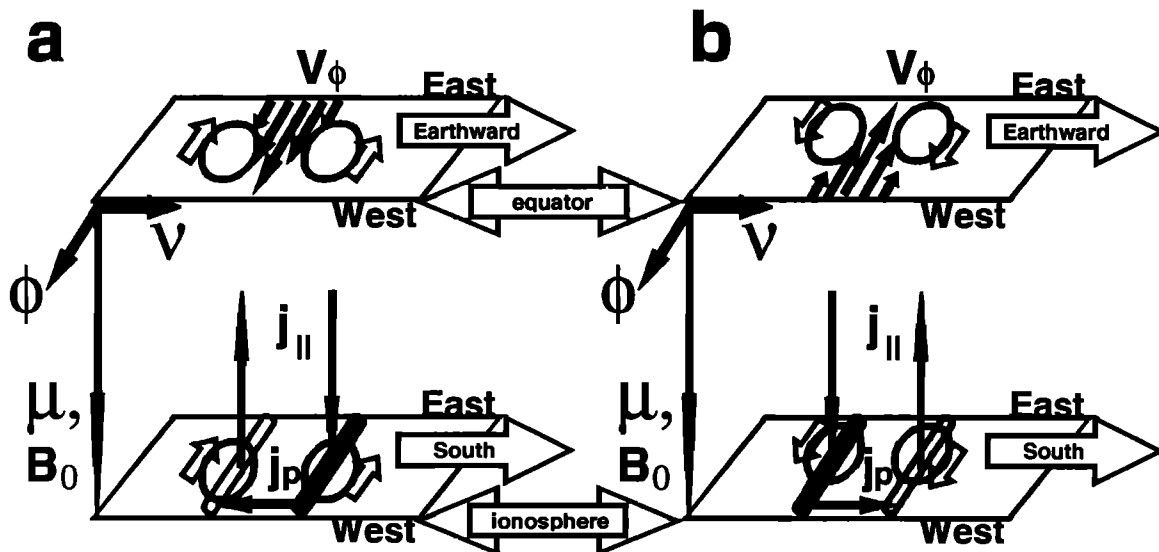


Figure 10. Schematic illustrating field-aligned current dynamics above the northern ionosphere due to the FLR and KH modes. During the first half of the FLR period when the FLR channel flow in the equatorial plane is (a) westward, this flow drives azimuthally stretched field-aligned currents upward where V_ϕ increases earthward and downward where V_ϕ decreases earthward. During the second half of period when the flow is (b) eastward, these field-aligned currents change positions. The KH mode wraps these regions as shown by circles with open arrows. Note that a ground-based observer will find that downward currents always wrap clockwise whereas upward currents wrap counterclockwise.

half period; namely, the upward field-aligned current wraps counterclockwise and the downward field-aligned current wraps clockwise. This schematic shows that visible ionospheric response does not depend on the SAW phase when the KH mode is activated.

One final point that we would like to emphasize is that the ionospheric electric field associated with FLRs cannot be geometrically mapped to the equatorial plane. This geometric mapping is only valid for processes with timescales much larger than Alfvén transit timescales along magnetic field lines. For example, typical FLRs can have field-aligned currents of the order of $5 \mu\text{A m}^{-2}$ near the ionosphere. For the height-integrated conductivities, we have assumed above ($\Sigma_P > 10 \text{ S}$), the ionospheric electric field would be of the order of 5 mV m^{-1} for the transverse scale of the order of 10 km ($E_{\text{ion}} \sim j_{\parallel} a / \Sigma_P$, where a is a transverse size of the j_{\parallel} region). A geometric mapping of this field to the equatorial plane gives an electric field of the order of 0.1 mV m^{-1} , which is smaller than the actual electric field associated with the equatorial plane of the FLR. These fields must be computed from the eigenmode solutions for the FLRs [see, i.g., Taylor and Walker, 1984].

5. Summary

The scenario of the vortex formation and evolution in the large-amplitude FLR on the dipolar magnetic field lines can be summarized as follows: The large-amplitude FLR, which is a linearly stable toroidal SAW, can be nonlinearly unstable with respect to the excitation of the KH mode in the equatorial magnetosphere. Initially, the full 3-D KH instability evolves in a fashion similar to the 2-D KH instability. However, the 3-D KH instability has a lower growth rate and a lower frequency at the equatorial plane. This difference occurs because of the field-aligned coupling and energy exchange between vortices at different altitudes along the field line. The analytical model predicts that the KH mode frequency correction is of the order of the FLR frequency. This result is in agreement with numerical modeling. Growth of the KH mode initiates perturbations in both azimuthal and radial components of the magnetic field. The exponential growth of magnetic field components starts at $\sim T/4$ when the KH vortex at the equator saturates. The magnetic perturbation achieves its maximum at $T/2$. At this time, amplitudes of field-aligned currents due to the KH and FLR modes become approximately of the same magnitude. For our parameters, the maximum of the azimuthally structured KH mode field-aligned current is $\sim 1.6 \mu\text{A m}^{-2}$ at the LAB, which is $1 R_E$ above the ionosphere, in this model. This value approximately equals to one half of the initial field-aligned current in the FLR. The field-aligned currents associated with the KH mode lead to wrapping of the field-aligned structure above the ionosphere. Time delay between the maxima of the KH mode velocity field and field-aligned currents above the ionosphere is close to $T/4$, which corresponds to the Alfvén transit time from the equatorial plane. In our model, the KH mode extracts $\sim 10\%$ of the FLR initial

energy during the first half of the SAW period. During the second half of the SAW period, a new vortex forms in a similar fashion as a primary vortex. However, this vortex is of the opposite direction to the initial one, and therefore it grows to lower amplitude. Finally, these two vortices cancel one another, which brings the kinetic energy from the KH mode back to the main SAW flow. This scenario implies that appearance and decay of vortices in the FLR may occur periodically, which corresponds to a periodical excitation and fading of auroral structures.

Finally, we have shown that the ionospheric footprint of field-aligned current dynamics predicted by the model does not depend on the initial phase of the SAW when the KH mode starts growing. Namely, the ground-based observer in the Northern Hemisphere (looking antiparallel to the Earth's magnetic field) will see the clockwise wrapping of the downward current and counterclockwise wrapping of the upward current.

Acknowledgments. This research was supported by the Natural Sciences and Engineering Research Council of Canada (NSERC), the Canadian Space Agency, and the Russian Foundation for Fundamental Research.

Janet G. Luhmann thanks Gerhard Haerendal and another referee for their assistance in evaluating this paper.

References

- Allan, W., and F.B. Knox, A dipole field model for axisymmetric Alfvén waves with finite ionosphere conductivities, *Planet. Space Sci.*, **27**, 79, 1979.
- Davis, T. N., and T. J. Hallinan, Auroral spirals, 1, Observations, *J. Geophys. Res.*, **81**, 3953, 1976.
- Galinsky, V. L., and B. U. O. Sonnerup, Dynamics of shear velocity layer with bent magnetic field lines, *Geophys. Res. Lett.*, **21**, 2247, 1994.
- Ganguli, G., Y. C. Lee, and P. J. Palmadesso, Kinetic theory for electrostatic waves due to transverse velocity shears, *Phys. Fluids*, **31**, 823, 1988.
- Haerendel, G., B. U. Olipitz, S. Buchert, O. H. Bauer, E. Rieger, and C. La Hoz, Optical and radar observations of auroral arcs with emphasis on small-scale structures, *J. Atmos. Terr. Phys.*, **58**, 71, 1996.
- Hallinan, T. J., Auroral spirals, 2, Theory, *J. Geophys. Res.*, **81**, 3959, 1976.
- Hallinan, T. J., and T. N. Davis, Small-scale auroral arc distortions, *Planet. Space Sci.*, **18**, 1735, 1970.
- Huba, J. D., Finite Larmor radius magnetohydrodynamics of the Rayleigh-Taylor instability, *Phys. Plasmas*, **3**, 2523, 1996.
- Lysak, R. L., Theory of auroral zone PiB pulsation spectra, *J. Geophys. Res.*, **93**, 5942, 1988.
- Lysak, R. L., Feedback instability of the ionospheric resonant cavity, *J. Geophys. Res.*, **96**, 1553, 1991.
- Lysak, R. L., and C. W. Carlson, The effect of microscopic turbulence on magneto-sphere-ionosphere coupling, *Geophys. Res. Lett.*, **8**, 269, 1981.
- Lysak, R. L., and W. Lotko, On the kinetic dispersion relation for shear Alfvén waves, *J. Geophys. Res.*, **101**, 5085, 1996.
- Miura, A., Stabilization of the Kelvin-Helmholtz instability by the transverse magnetic field in the magnetosphere-ionosphere coupling system, *Geophys. Res. Lett.*, **23**, 761, 1996.

- Miura, A., and J. R. Kan, Line-tying effects on the Kelvin-Helmholtz instability, *Geophys. Res. Lett.*, *19*, 1611, 1992.
- Miura, A., and P. L. Pritchett, Nonlocal stability analysis of the MHD Kelvin-Helmholtz instability in a compressible plasma, *J. Geophys. Res.*, *87*, 7431, 1982.
- Petviashvili, V. I., and O. A. Pokhotelov, Dipole Alfvén vortices, *Sov. Phys. JETP, Engl. Transl.*, *42*, 54, 1985.
- Rankin, R., B. G. Harrold, J. C. Samson, and P. Frycz, The nonlinear evolution of field line resonances in the Earth's magnetosphere, *J. Geophys. Res.*, *98*, 5839, 1993.
- Rankin, R., P. Frycz, J. C. Samson, and V. T. Tikhonchuk, Shear flow vortices in magnetospheric plasmas, *Phys. Plasmas*, *4*, 829, 1997.
- Rankin, R., J. C. Samson, V. T. Tikhonchuk, and I. Voronkov, Auroral density fluctuations on dispersive field line resonances, *J. Geophys. Res.*, *104*, 4399, 1999.
- Samson, J. C., L. L. Cogger, and Q. Pao, Observations of field line resonances, auroral arcs, and auroral vortex structures, *J. Geophys. Res.*, *101*, 17373, 1996.
- Samson, J. C., R. Rankin, and I. Voronkov, Field line resonances, auroral arcs, and substorm intensifications, in *Geospace Mass and Energy Flow: Results From the International Solar-Terrestrial Physics Program*, *Geophys. Monogr. Ser.*, vol. *104*, edited by J. L. Hortwitz et al., p. 161, AGU, Washington, D. C., 1998.
- Southwood, D. J., and W. J. Hughes, Theory of hydromagnetic waves in the magnetosphere, *Space Sci. Rev.*, *35*, 301, 1983.
- Strauss, H. R., Nonlinear, three-dimensional magnetohydrodynamics of noncircular tokamaks, *Phys. Fluids*, *19*, 134, 1976.
- Streltsov, A., and W. Lotko, The fine structure of dispersive, nonradiative field line resonance layers, *J. Geophys. Res.*, *101*, 5343, 1996.
- Streltsov, A. V., and W. Lotko, Dispersive, nonradiative field line resonances in a dipolar magnetic field geometry, *J. Geophys. Res.*, *102*, 27121, 1997.
- Tajima, T., W. Horton, P. J. Morrison, J. Schutkeker, T. Kamimura, K. Mima, and Y. Abe, Instabilities and vortex dynamics in shear flow of magnetized plasmas, *Phys. Fluids B*, *3*, 938, 1991.
- Taylor, J. P. H., and A. D. M. Walker, Accurate approximate formulae for toroidal standing hydromagnetic oscillations in a dipolar geomagnetic field, *Planet. Space Sci.*, *32*, 1119, 1984.
- Thomas, V. A., and D. Winske, Kinetic simulations of the Kelvin-Helmholtz instability at the magnetopause, *J. Geophys. Res.*, *98*, 11425, 1993.
- Trakhtengertz, V. Y., and A. Y. Feldstein, Quite auroral arcs: Ionosphere effect of magnetospheric convection stratification, *Planet. Space Sci.*, *32*, 127, 1984.
- Trakhtengertz, V. Y., and A. Y. Feldstein, Turbulent Alfvén boundary layer in the polar ionosphere, 1, Excitation conditions and energetics, *J. Geophys. Res.*, *96*, 19363, 1991.
- Trondsen, T. S., and L. L. Cogger, High-resolution television observations of black aurora, *J. Geophys. Res.*, *102*, 363, 1997.
- Trondsen, T. S., and L. L. Cogger, A survey of small-scale spatially periodic distortions of auroral forms, *J. Geophys. Res.*, *103*, 9405, 1998.
- Voronkov, I., R. Rankin, V. T. Tikhonchuk, and J. C. Samson, Nonlinear shear Alfvén resonances in a dipolar magnetic field, *J. Geophys. Res.*, *102*, 27137, 1997a.
- Voronkov, I., R. Rankin, P. Frycz, V. T. Tikhonchuk, and J. C. Samson, Coupling of shear flow and pressure gradient instabilities, *J. Geophys. Res.*, *102*, 9639, 1997b.
- Wei, C. Q., J. C. Samson, R. Rankin, and P. Frycz, Electron inertia effects on geomagnetic field line resonances, *J. Geophys. Res.*, *99*, 11265, 1994.

R. Rankin, J. C. Samson, V. T. Tikhonchuk, and I. Voronkov, Department of Physics, University of Alberta, Edmonton, Alberta, Canada, T6G 2J1. (e-mail: igor@space.ualberta.ca)

(Received December 7, 1998; revised March 22, 1999; accepted April 6, 1999.)